Drug Design, Development and Therapy

Dovepress
Taylor & Francis Group

Open Access Full Text Article

ORIGINAL RESEARCH

Identification of Key Genes in Esketamine's Therapeutic Effects on Perioperative Neurocognitive Disorders via Transcriptome Sequencing

Wen Hu[1,*], Jieqiong Luo[1,*], Hui Li[2,*], Yushan Luo[1,*], Xiaoyuan Zhang[1], Zhen Wu[1], Qian Yang[1], Sirun Zhao[1], Bailong Hu[2], Xiaohua Zou[2]

[1]Guizhou Medical University, Guiyang, Guizhou, 550004, People's Republic of China; [2]Department of Anesthesiology, The Affiliated Hospital of Guizhou Medical University, Guiyang, Guizhou, 550004, People's Republic of China

*These authors contributed equally to this work

Correspondence: Bailong Hu; Xiaohua Zou, Department of Anesthesiology, Affiliated Hospital of Guizhou Medical University, Guiyang City, Guizhou Province, People's Republic of China, Tel +86-15185184309; +86-13809416036, Fax +86-851-86771013, Email 375896605@qq.com; zouxiaohuazxh@163.com

Background: Esketamine ameliorates propofol-induced brain damage and cognitive impairment in mice. However, the precise role and underlying mechanism of esketamine in perioperative neurocognitive disorders (PND) remain unclear. Therefore, this study aimed to investigate the key genes associated with the role of esketamine in PND through animal modeling and transcriptome sequencing.

Methods: The present study established a mice model of PND and administered esketamine intervention to the model, and mice were divided into control, surgical group, and surgical group with esketamine. Behavioral assessments were conducted using the Morris water maze and Y maze paradigms, while transcriptome sequencing was performed on hippocampal samples obtained from 3 groups. Differential expression analysis and weighted gene co-expression network analysis (WGCNA) were performed on sequencing data to identify candidate genes related to esketamine treating PND. Thereafter, protein-protein interaction (PPI) network analysis was implemented to select key genes. The genes obtained from each step were subjected to enrichment analysis, and a regulatory network for key genes was constructed.

Results: The Morris water maze and Y maze findings demonstrated the successful construction of our PND model, and indicated that esketamine exhibits a certain therapeutic efficacy for PND. Ank1, Cbln4, L1cam, Gap43, and Shh were designated as key genes for subsequent analysis. The 5 key genes were significantly enriched in cholesterol biosynthesis, nonsense mediated decay (NMD), formation of a pool of free 40s subunits, major pathway of rRNA processing in the nucleolus and cytosol, among others. Notably, the miRNAs, mmu-mir-155-5p and mmu-mir-1a-3p, functionally co-regulated the expression of Ank1, Gap43, and L1cam.

Conclusion: We uncovered the therapeutic efficacy of esketamine in treating PND and identified 5 key genes (Ank1, Cbln4, L1cam, Gap43, and Shh) that contribute to its therapeutic effects, providing a valuable reference for further mechanistic studies on esketamine's treatment of PND.

Keywords: esketamine, perioperative neurocognitive disorders, key genes, transcriptome sequencing

Introduction

More than 300 million surgeries are conducted worldwide annually, with a continuing increase.[1] Perioperative neurocognitive disorder (PND) is a frequent complication caused by anesthesia and surgical interventions impacting the central nervous system, commonly observed in elderly patients, with incidence rates reported to be between 15% and 60%.[2,3] PND predominantly presents as changes in cognitive functions, including memory impairment and decreased attentional capacity, in more severe instances, individuals may exhibit personality alterations and reduced social functioning.[4] PND

Received: 18 December 2024
Accepted: 5 February 2025
Published: 14 February 2025

can greatly affect postoperative quality of life, increase healthcare costs, extend hospital stays, and potentially raise mortality rates, burdening families and society.[5] Although research has identified hippocampal neuroinflammation, synaptic dysfunction, blood-brain barrier (BBB) damage, oxidative stress, and neuronal damage as primary characteristics of PND,[6–9] the precise underlying mechanisms remain elusive. Additionally, there is a notable deficiency in early biomarkers and effective treatment strategies. Consequently, it is imperative to conduct in-depth investigations into the key genes associated with PND, elucidate the potential molecular mechanisms, and promote the development of novel therapeutic approaches.

Esketamine is a non-competitive antagonist of the N-methyl-D-aspartate (NMDA) receptor. Compared to ketamine, it has a higher affinity for the NMDA receptor, provides stronger anesthetic effects, fewer side effects, and better antidepressant efficacy, with a clinical dose that is only half of that required for ketamine.[10] As a general anesthetic, esketamine has recently garnered widespread attention for its use in modulating cognitive function during the perioperative period.[11] Research suggests that intraoperative administration of low-dose esketamine (0.25 mg/kg loading dose, 0.125 mg/kg/h infusion) may modestly reduce the incidence of delayed neurocognitive recovery (DNR) and cardiovascular adverse events in elderly patients undergoing general anesthesia for gastrointestinal tumor surgeries.[12] Additionally, another study has demonstrated that administering a subanesthetic dose of esketamine (0.15 mg/kg) can mitigate delayed neurocognitive recovery and improve early postoperative cognitive function in elderly patients undergoing gastrointestinal surgery, likely due to its anti-neuroinflammatory properties.[13] Furthermore, research has shown that esketamine alleviates isoflurane-induced cognitive impairment and brain damage in rats by activating the mBDNF/TrkB/PI3K signaling pathway.[14] In summary, esketamine shows promise as an effective treatment for perioperative neurocognitive disorders, however, its specific mechanisms remain unclear.

This study utilizes an in vivo PND mouse model to investigate key genes and potential mechanisms associated with esketamine treatment for PND. By employing transcriptomic data analysis, differential expression analysis, weighted gene co-expression network analysis (WGCNA), and protein-protein interaction (PPI) network construction, we aim to identify relevant genes. Furthermore, enrichment analysis and regulatory network construction were conducted to elucidate the roles of these genes in the context of perioperative neurocognitive disorders, thereby providing a foundational basis for assessing the efficacy of esketamine treatment.

Materials and Methods

Animal Modeling

A number of 18 18-month-old male C57BL/6J mice (25g-35g) were purchased from Phenotek Biotechnology (Shanghai) Co.,Ltd. (SCXK(hu)2018–0005). The Animal Center of Guizhou Medical University granted approval for the experimental protocol (2305211), and all procedures were conducted following the guidelines provided by the National Institutes of Health Guide for the Care and Use of Laboratory Animals. The animals were randomly allocated into three groups (control, surgical, and surgical group with esketamine), with each group comprising of 6 male mice. The animals were maintained at a constant temperature of 20–25°C under a light/dark cycle of 12/12 hours, with ad libitum access to food and water. An exploratory laparotomy was performed under sterile conditions using sevoflurane anesthesia (3–5% for induction and 1.5–2.5% for maintenance) to simulate abdominal exploratory surgery in C57BL/6J mice.[15] The abdomen was first disinfected with 75% ethanol. A vertical incision, approximately 1.5–2 cm in length, was made about 0.5 cm below the right lower rib to gain access to the abdominal cavity. The internal organs and muscle tissue were gently manipulated using the index finger. Approximately 3–5 cm of intestine was then carefully exteriorized and vigorously rubbed between the thumb and forefinger for 30 seconds. Afterward, the intestine was carefully repositioned into the peritoneal cavity, and the abdominal wall was closed in layers. The entire procedure lasted approximately 30 minutes. In the sham-operated group, animals were anesthetized for the same duration as those in the surgical group, but their abdomens were only disinfected, with no incisions made. Esketamine (10 mg/kg) dissolved with saline (0.9%) was injected intraperitoneally immediately after PND.[16] The mice were euthanized following anesthesia, and the hippocampal tissues were harvested. Meanwhile, the serum levels of TNF-α and IL-6 were quantified using a mouse

tumor necrosis factor α (TNF-α) ELISA kit (MEIMIAN, Jiangsu) and a mouse interleukin-6 (IL-6) ELISA kit (MEIMIAN) in blood samples. All cognitive function tests were conducted under well-lit conditions.

Morris Water Maze

The Morris water maze experiment comprised navigation training and memory testing. We used a water labyrinth system of the brand Shanghai Xinruan (model XR-XM101, swimming pool: diameter 1.2 meters, height 45 cm, manual lifting platform: diameter 8 cm) for the test. Firstly, a two-day acclimatization training was conducted, where mice were placed into the water maze without platforms and swam freely for about 60 seconds, and 120 seconds on the second day. Next, mice underwent 5 days of training, including three periods (swimming training with a visible platform, swimming training with a hidden platform, and a probe trial). On the first day, the mice received four swim training sessions, with a visible platform in one quadrant of the pool. From day 2 to day 5, the mice underwent orientation and navigation training with a hidden platform in the same quadrant of the pool, with two 60-second training sessions per day. The training lasted for 4 days, with a total of 8 sessions, each session spaced at least 4 hours apart. During the training, after the mice successfully found the platform, they were allowed to stay on the platform for 10–15 seconds. If the mice did not find the platform within 60 seconds, the experimenter guided them to stay on the platform for 10–15 seconds. Finally, the probe trial was conducted on the first and third days after anesthesia. The activity duration and path of mice in the quadrant where the initial platform was positioned were recorded (the mice entered water in quadrant one, while an escape platform was situated in quadrant three; data regarding incubation period upon reaching this escape platform by mice was collected). The data were analyzed by *t* test using Prism10.1.2 software.

Y-Maze

The mice were acclimatized to the laboratory environment for a minimum of one day prior to the formal experiment in order to mitigate stress response. Gently place the mice in the central area of the Y maze, with any arm selected as the starting position. The mice were allowed unrestricted exploration of the maze, and typically, the duration of each experiment ranged from 5 to 10 minutes. Throughout the experiment, the left arm was designated as the target arm, and data on both entry frequency into this specific arm and total attempts were collected. Completion rate = (Number of frequency into left arm / Number of total attempts) x 100%. We used the Shanghai Xinruan brand Y maze device (model XR-XY1032; Y-shaped compartment 21×7 × 15.5 cm, three arms of equal length) for the test. The data were analyzed by *t* test using Prism10.1.2 software.

Histopathological Analysis

Collection of 2 hippocampal tissue and blood samples were collected after the probe trial was completed. In one copy, the hippocampal tissues were rinsed with PBS and then immersed in a fixative solution containing 4% paraformaldehyde for a period of 24–48 hours. Following fixation, the tissues underwent standard paraffin embedding techniques for further processing. Thin sections measuring 5 μm in thickness were prepared and subjected to hematoxylin and eosin (HE) staining, enabling visualization of histopathological morphology using a microscope. Another copy, which was preserved using RNA protection solution (transferred overnight at 4°C to - 80°C for storage in the refrigerator).

Transcriptome Sequencing

Total RNA of 18 hippocampal tissues from 3 groups was isolated and purified from samples using TRIzol (Invitrogen, CA, USA) according to the manufacturer's protocol. The quantity and purity of total RNA were assessed using NanoDrop ND-1000 (NanoDrop, Wilmington, DE, USA). RNA integrity was evaluated using Bioanalyzer 2100 (Agilent, CA, USA), and validation was performed via agarose gel electrophoresis. Samples meeting the criteria of concentration >50 ng/μL, RIN value >7.0, OD260/280 >1.8, and total RNA >1 μg were used for downstream experiments. Polyadenylated mRNA was specifically captured using oligo (dT) magnetic beads (Dynabeads Oligo (dT), Thermo Fisher, USA) through two rounds of purification. The captured mRNA was fragmented at high temperature using the NEBNext® Magnesium RNA Fragmentation Module (NEB, USA), at 94°C for 5–7 minutes. Fragmented RNA was reverse transcribed into cDNA using Invitrogen SuperScript™ II Reverse Transcriptase (Invitrogen). Next, double-

stranded synthesis was performed using E. coli DNA polymerase I (NEB) and RNase H (NEB) to convert the DNA-RNA duplex into double-stranded DNA, with incorporation of dUTP Solution (Thermo Fisher) to blunt the ends. A single A base was added to each end to facilitate ligation with adapters carrying a terminal T base. The library was size-selected and purified using magnetic beads. The double-stranded DNA was then digested with UDG enzyme (NEB). The DNA library was PCR-amplified under the following conditions: initial denaturation at 95°C for 3 minutes; 8 cycles of denaturation at 98°C for 15 seconds, annealing at 60°C for 15 seconds, and extension at 72°C for 30 seconds; final extension at 72°C for 5 minutes, resulting in a library with fragment sizes of 300 bp ± 50 bp. Finally, the library was subjected to paired-end sequencing using Illumina Novaseq™ 6000 (LC Bio Technology CO., Ltd., Hangzhou, China) according to standard protocols, with a sequencing mode of PE150.

Data Processing

The distribution of base types was utilized for the detection of AT and GC separation. The mouse gene annotation file was utilized as the reference gene set, followed by data processing to obtain count data. Subsequently, a principal component analysis (PCA) map was generated to visualize the principal components between samples.

Differential Expression Analysis

The differential expression analysis between the sample expression matrix of the surgical group and the control group, as well as between the surgical group with esketamine and surgical group, was performed utilizing the DESeq2 package (V 1.38.0).[17] A significance level of $P < 0.05$ and $|\log_2\text{fold change (FC)}| > 0.5$ were applied to identify differentially expressed genes (DEGs). In order to comprehensively analyze the distribution of DEGs, we utilized the ggplot2 package (V 3.4.4)[18] to generate a volcano plot for visualizing these genes. The volcano plot highlighted the top 10 up-regulated and down-regulated genes based on their $\log_2$FC values. Additionally, the pheatmap package (V 1.0.12)[19] was employed to create a heatmap specifically showcasing the expression level of these 20 genes. The DEGs in the surgical group and control groups were referred to as DEGs1, while the DEGs in the surgical group with esketamine and surgical groups were denoted to as DEGs2. The intersection genes related to PND treatment were selected by intersecting the genes exhibiting opposite expression trends in DEGs1 and DEGs2.

Weighted Gene Co-Expression Network Analysis (WGCNA)

Using the WGCNA package (v 1.71),[20] WGCNA was conducted on all sample expression matrices to identify PND- and esketamine treatment-associated module genes. The initial step involved clustering all the samples and utilizing Euclidean distance of the gene expression level for conducting hierarchical clustering. This process aimed to identify any potential outliers within the samples, which should subsequently be eliminated. Thereafter, the relationship between the soft threshold β and the scale-free network evaluation coefficient R^2, as well as the mean connectivity, was established. The β was determined by setting R^2 to be greater than 0.9 and ensuring that the mean connectivity was close to 0. The scale-free network was constructed according to the selected β. All genes in this network were divided into several modules by setting the minimum gene number of each module to 200, the deepSplit to 4, and the mergeCutHeight to 0.25, and then partitioned with different colors. The Pearson correlation coefficient was computed to determine the relationship between these modules and the surgical group as well as the surgical group with esketamine. Subsequently, the module exhibiting strong correlations with both phenotypes was identified as the key module ($|\text{cor}| > 0.4$, $P < 0.05$), from which key module genes were extracted. Afterwards, the intersection genes related to PND treatment were crossed with these key module genes to determine candidate genes.

Enrichment Analysis and Correlation Analysis

The clusterProfiler package (V 4.7.1.003)[21] was utilized to perform Gene Ontology (GO) function and Kyoto Encyclopedia of Genes and Genomes (KEGG) enrichment analyses on intersection genes and candidate genes, respectively, aiming to investigate the biological functions and signaling pathways associated with these genes ($P < 0.05$). In order to further investigate the correlation and expression of candidate genes and synaptic/complement related pathways, the genes located in the relevant pathways identified by candidate genes were extracted. Subsequently, their single sample

gene set enrichment analysis (ssGSEA) scores were computed, and the scores differences among groups were illustrated ($P < 0.05$). The correlation analysis between pathway-related genes and candidate genes was subsequently conducted, followed by the generation of an expression heat map depicting these genes in the samples.

Protein-Protein Interaction (PPI) Network Analysis

In order to comprehend the interaction among corresponding proteins of the candidate genes, they were inputted into the Search Tool for the Retrieval of Interacting Genes/Proteins (STRING) database (http://www.string-db.org/) with an interaction score greater than 0.15. The PPI network was visualized adopting Cytoscape software (V 3.9.1).[22] Subsequently, the Degree algorithm in cytoHubba plug-in was employed to further screen candidate genes that exhibit protein-level interactions. The key genes were recorded as the top 5 most significant genes identified by the Degree algorithm. The expression levels of key genes in the dataset among the three groups were visualized applying violin plots to elucidate biomarker expression. Additionally, Wilcoxon test was employed to compare and calculate the *P* of significance among the groups ($P < 0.05$).

Gene Set Enrichment Analysis (GSEA)

Then key genes were subjected to clusterProfiler package for GSEA to explore pathways in which they participated, with the m2.cp.v2023.1.Mm.symbols.gmt as reference gene sets from the Molecular Signatures Database (MSigDB, https://www.gsea-msigdb.org/gsea/msigdb) ($P < 0.05$). In particular, for key genes, their correlations with other genes of samples were calculated using the Spearman algorithm in the psych package (V 2.2.9)[23] and sequenced for GSEA.

Construction of Network

In order to dig potentially regulation mechanism of key genes and provide references for investigating the molecular mechanism of esketamine therapy for PND, transcription factors (TFs) that may have regulatory roles in key genes expression were predicted utilizing the transcriptional regulatory relationships unravelled by sentence-based text-mining (TRRUST) database (http://www.grnpedia.org/trrust). The resulting TF-gene network was constructed employing Cytoscape software. After that, an analysis was performed to search for functions in which these key genes and their predicted TFs were involved via the Metascape database (https://metascape.org/gp/index.html#/main/step1). Similarly, the TRRUST database was used to predict the upstream microRNAs (miRNAs) of key genes. Finally, TF/miRNA-gene regulatory network was constructed.

Reverse Transcription Quantitative Polymerase Chain Reaction (RT-qPCR)

To investigate variations in key genes expression across different groups, we collected six tissue samples from each group (control, surgical, and surgical group with esketamine), for RT-qPCR analysis. The TRIzol reagent (Ambion, Austin, USA) was utilized for the extraction of total RNA according to the manufacturer's purification protocol. Following that, the SureScript First-strand cDNA synthesis kit (Servicebio, Wuhan, China) was employed to perform reverse transcription and generate cDNA from the isolated RNA. The cDNA obtained was subsequently subjected to analysis using 2xUniversal Blue SYBR Green qPCR Master Mix (Servicebio) along with specific primers (Supplementary Table 1). The RT-qPCR amplification process was conducted with the following thermal cycling conditions: an initial denaturation step at 95°C for a duration of 1 minute, followed by 40 cycles consisting of denaturation at 95°C for a period of 20 seconds, annealing at 55°C for a duration of 20 seconds, and extension at 72°C for a period of 30 seconds. Data analysis was conducted utilizing the $2^{-\Delta\Delta Ct}$ approach, where GAPDH was employed as the internal reference gene for standardization purposes.

Statistical Analysis

Bioinformatics analyses were conducted using R language (v. 4.2.2); DESeq2 analysis of sample expression matrix based on differential expression between different groups of samples; data from different groups were compared using the Wilcoxon test ($P < 0.05$); the spearman algorithm calculated the correlation; the experimental design employed one-way ANOVA to evaluate the differences among groups, and the results were presented in the form of mean ± SD.

Results

Evaluation of Animal Models

The experimental flow of animal model construction was shown in Figure 1A. Figure 1B and Supplementary Figures 1−3 showed the representative swimming trajectories of the mice in each group on the last day of training and testing. In the

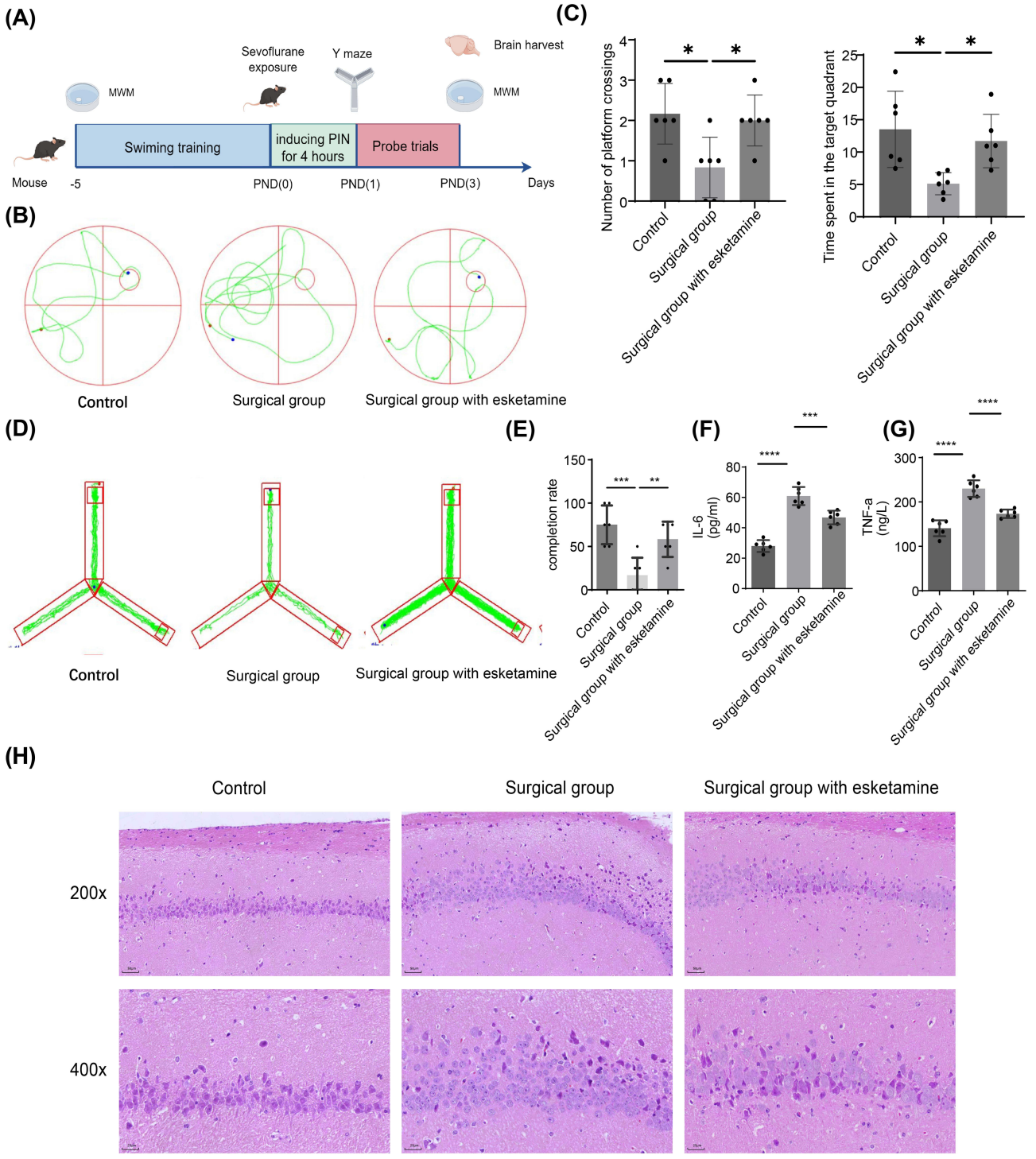

Figure 1 Esketamine improves cognitive dysfunction in PND mice. (**A**) The experimental flow of animal model construction. (**B**) Representative movement trajectories of each group of mice on the last day of the MWM test. (**C**) Number of platform crossings and time spent in the target quadrant during the testing phase of the MWM test for each group. * represented $p < 0.05$. (**D**) Representative movement trajectories of each group of mice on the Y-maze test. (**E**) Task completion rate in the Y-maze for mice in each group. * represented $p < 0.05$, ** represented $p < 0.01$. (**F**) Expression levels of IL-6 in the serum of mice from each group. *** represented $p < 0.001$. (**G**) Expression levels of TNF-α in the serum of mice from each group. **** represented $p < 0.0001$. (**H**) Representative images of HE-stained hippocampal sections from mice in each group. n = 6.

https://doi.org/10.2147/DDDT.S510752

Morris water maze, the surgical group exhibited a significant reduction in the time spent within the target quadrant and a decreased frequency of platform crossings compared to the control group; the intervention group spent significantly more time in the target quadrant and crossed the plateau significantly more often compared to the surgical group. ($P < 0.05$) (Figure 1C). In addition, Y-maze experiments revealed significant differences in task completion rates between the control and surgical groups, as well as between surgical group and surgical group with esketamine ($P < 0.05$), with the control and surgical group with esketamine demonstrating superior performance compared to the surgical group (Figure 1D and E). Moreover, the levels of IL-6 and TNF-α in the serum were significantly elevated in the surgical group compared to the control group, while they were significantly reduced in the intervention group compared to the surgical group (Figure 1F and G). In the hippocampal tissue of the control group, the neurons exhibited a complete and orderly structure with distinct outlines. Conversely, in the surgical group, there was disarray in the arrangement of hippocampal neurons, accompanied by cellular swelling and an unclear structural appearance. Additionally, neuron loss was observed. Comparatively, mice in the surgical group with esketamine displayed relatively intact neuronal structures with organized arrangements and clear outlines; instances of neuron loss were infrequently observed (Figure 1H). The above findings demonstrated the successful construction of our PND model, and indicated that esketamine exhibits a certain therapeutic efficacy for PND.

Data Evaluation

The base proportion distribution of all samples was illustrated in Supplementary Figure 4. However, it should be noted that due to inherent limitations of the sequencing instrument itself, there may be slight fluctuations in the A/T and C/G contents of the initial bases. Nevertheless, these variations do not compromise the overall data quality. Furthermore, the sample comparison rate of all data exceeded 88% (Supplementary Table 2). PCA revealed no statistically significant outliers within each group of samples (Supplementary Figure 5).

Intersection Genes Related to PND Treatment

The surgical group and the control group exhibited 964 DEGs1, with 550 genes up-regulated and 414 genes down-regulated in the surgical group (Figure 2A and B). GSEA showed that the DEGs1 were significantly enriched in 13 pathways, which included the dopaminergic neurogenesis, G protein coupled receptors (GPCRS) nonodorant, and the Type II Interferon Signaling pathway (IFNG) (Figure 2C). The surgical group with esketamine and surgical group yielded 1787 DEGs2, comprising 703 up-regulated genes and 1084 down-regulated genes in surgical group with esketamine (Figure 2D and E). The DEGs2 existed enrichment in 19 pathways, containing cytoplasmic ribosomal proteins, GPCRS nonodorant, blood clotting cascade, etc. (Figure 2F). Interestingly, the GPCRS nonodorant was up-regulated in DEGs1 and down-regulated in DEGs2, suggesting that GPCRS nonodorant played a role in esketamine treatment of PND. By intersecting the genes exhibiting opposite expression trends in DEGs1 and DEGs2, 557 intersection genes related to PND treatment were selected (Figure 3A and B). GO enrichment analysis revealed 1138 terms were involved by intersection genes, encompassing 909 biological processes (BPs, eg signal release from synapse), 100 cellular components (CCs eg excitatory synapse), and 129 molecular functions (MFs, eg structural constituent of postsynapse) (Figure 3C, Supplementary Table 3). Additionally, the intersection genes were notably enriched in 47 KEGG signaling pathways, such as the Wnt signaling pathway - Mus musculus (house mouse) and the Phospholipase D signaling pathway - Mus musculus (house mouse) (Figure 3D, Supplementary Table 4).

Identification of Candidate Genes

The cluster analysis of WGCNA showed that there were no outliers (Figure 4A). When the R^2 was 0.921, the β was 8, and the network adhered to a scale-free distribution (Figure 4B). A number of 15 co-expression modules were identified, with the MEtan and MEyellow modules demonstrating had stronger correlation with the surgical group (cor = 0.54, 0.49, $P < 0.05$) and surgical group with esketamine (cor = −0.56, −0.6, $P < 0.05$), and thus were selected as the key modules (Figure 4C and D). The 2927 genes in these key modules were key module genes. Afterwards, the 577 intersection genes were crossed with these key module genes to identify 68 candidate genes (Figure 4E).

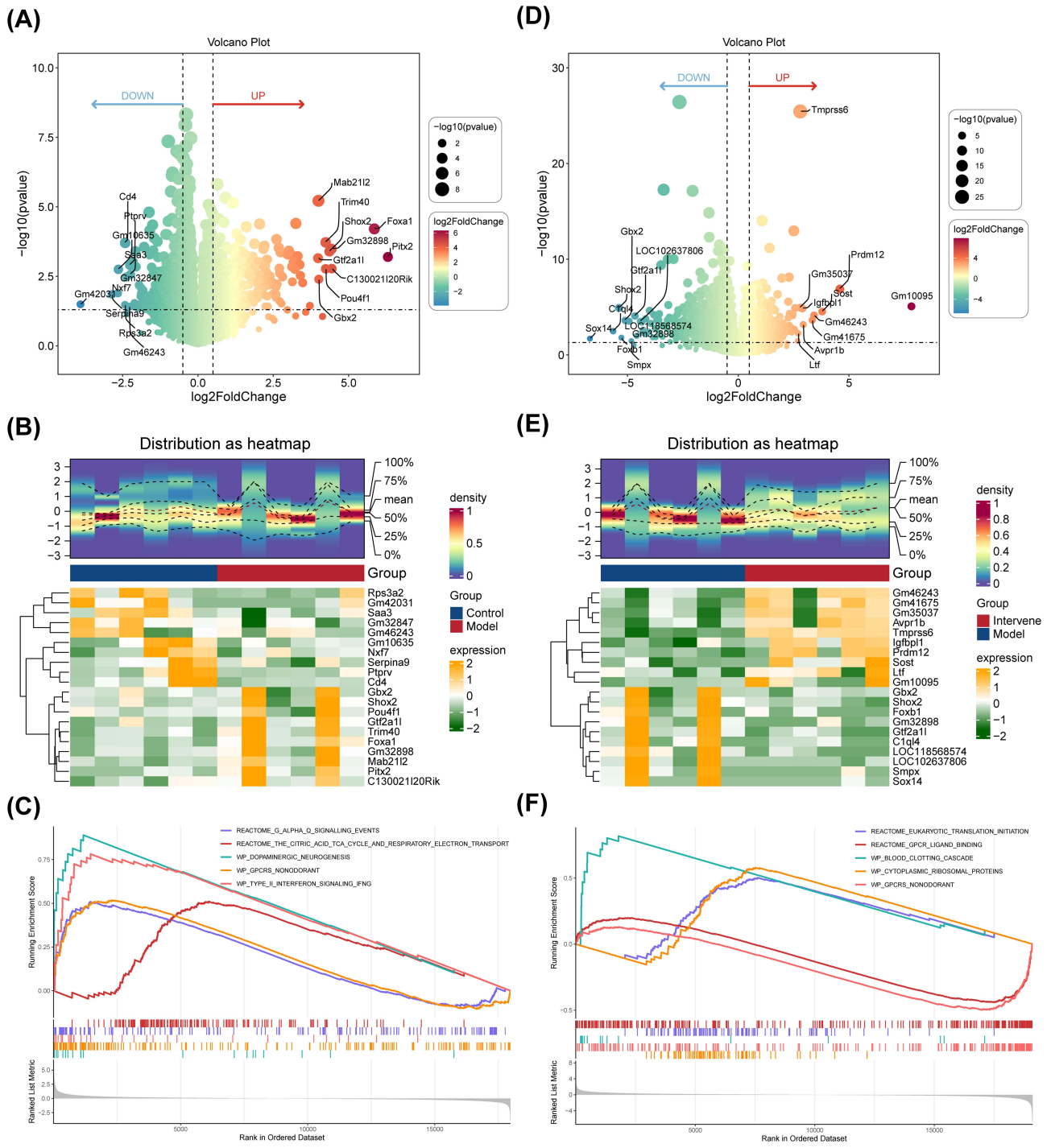

Figure 2 Identification and functional enrichment analysis of differentially expressed genes in the control, surgical, and surgical group with esketamine groups. (**A**) Volcano Plot of differentially expressed genes between control and surgical group. (**B**) Density Heatmap of differentially expressed genes between control and surgical group. (**C**) GSEA enrichment analysis plot for differentially expressed genes between control and surgical group (DEGs1). (**D**)Volcano Plot of differentially expressed genes between surgical group and surgical group with esketamine. (**E**) Density Heatmap of differentially expressed genes surgical group and surgical group with esketamine. (**F**) GSEA enrichment analysis plot for differentially expressed genes between model and surgical group with esketamine (DEGs2).

Synaptic Complement-Related Pathway Played Roles in PND Treatment by Esketamine

Following GO enrichment analysis of the candidate genes, 500 significant results were obtained, comprising 366 BPs, 57 CCs, and 77 MFs (Figure 5A, Supplementary Table 5). They were synapse organization, inhibitory synapse assembly, glycinergic synapse, etc. The KEGG pathways that enriched by candidate genes were axon guidance - Mus musculus (house

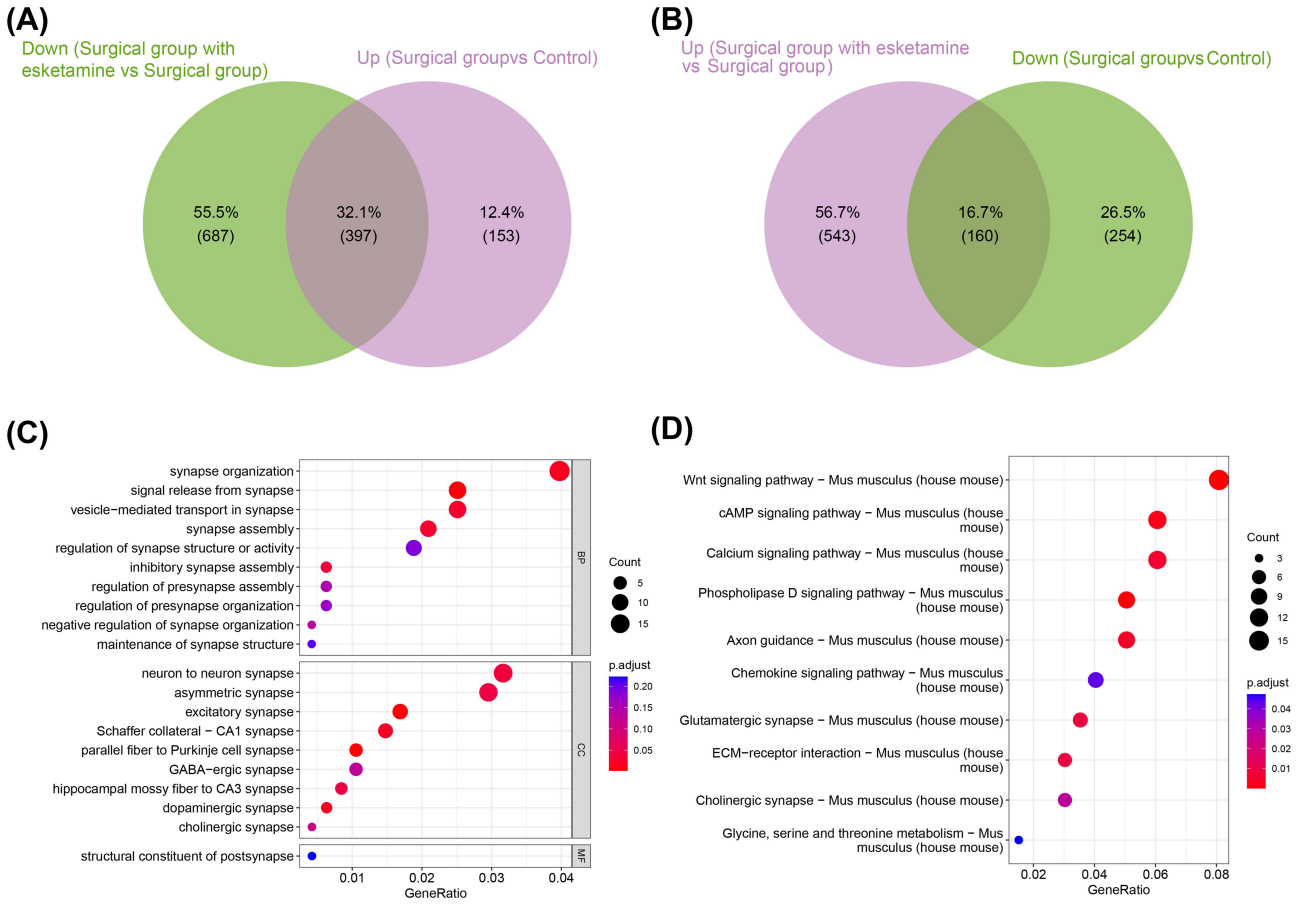

Figure 3 Identification and functional enrichment analysis of intersection genes related to PND treatment. (**A** and **B**) Venn diagram of the genes exhibiting opposite expression trends in DEGs1 and DEGs2. (**C**) GO comment results of intersection genes. (**D**) KEGG enrichment result of intersection genes.

mouse), Cholinergic synapse - Mus musculus (house mouse), and so on (Figure 5B, Supplementary Table 6). The aforementioned pathways pertain to synaptic and complement-related mechanisms. First, genes situated within the acquired synaptic and complement - related pathways were identified. During GO enrichment analysis, it was determined that Cbln4, Grin3a, Gpld1, Unc13c, Glra3, Cntnap4, L1cam, Gap43, Itga3, Lgi2, and Adgra1 were positioned within synaptic/complement - related pathways. Additionally, genes significantly associated with synaptic/complement - related pathways in KEGG analysis included L1cam, Camk2d, Shh, Epha8, and Kcnj12. The gene ssGSEA scores derived from both GO and KEGG analyses were computed independently. Notably, significant disparities in these scores were observed between the surgical group and the surgical group with esketamine, suggesting that the synaptic complement-related pathway played a crucial role in the therapeutic efficacy of esketamine during PND (Figure 5C and D). Additional analysis revealed a positive correlation between these genes and the majority of the candidate genes, with the complement-related genes (C1qa, C3, C3ar1, and C5ar1) demonstrating a strong positive correlation with the candidate genes (such as Itga3, Cdk18) (Figure 5E–G).

Ank1, Cbln4, L1cam, Gap43, and Shh Were Key Genes

The PPI network encompassed 47 nodes, with 21 genes identified as outliers not being mapped. The network exhibited 113 edges, and the mean node degree was calculated to be 4.19. The most important genes identified by the Degree algorithm, which were Ank1, Cbln4, L1cam, Gap43, and Shh, were designated as key genes for subsequent analysis (Figure 6A). There were significant differences in expression level of these key genes between the control and surgical groups, as well as between the surgical group and surgical group with esketamine, and it could be inferred that all key genes were up-regulated in the surgical group (Figure 6B). After drug surgical group with esketamine, there was a trend of decrease, which was in line with realistic logic. The 5 key genes were significantly enriched in cholesterol biosynthesis, nonsense mediated decay (NMD), formation of

https://doi.org/10.2147/DDDT.S510752

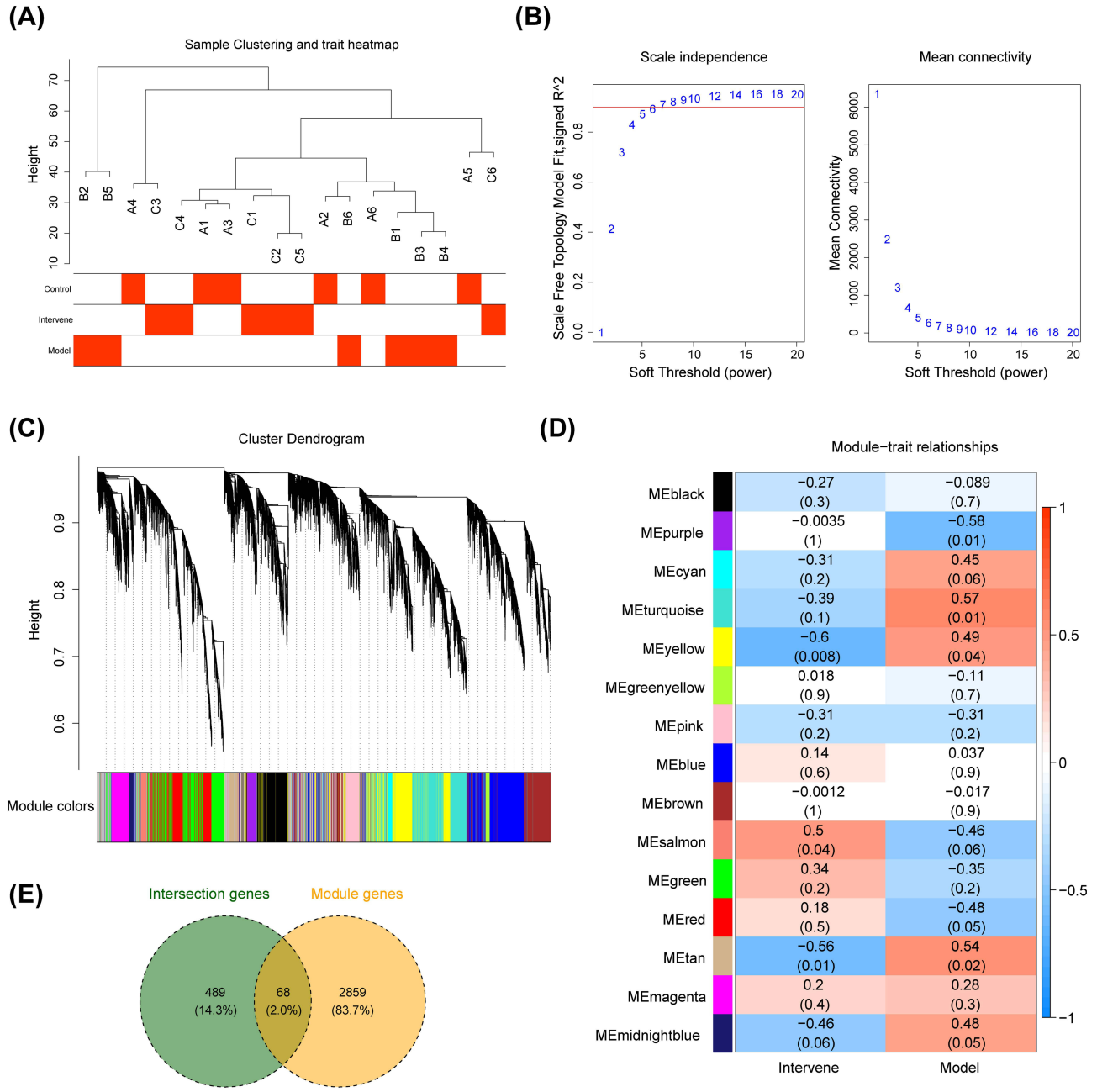

Figure 4 Weighted co-expression network analysis (WGCNA) analysis of identifying candidate genes. (**A**) Determination of sample hierarchical clustering in WGCNA analysis. (**B**) The soft threshold power and the mean connectivity of WGCNA. (**C**) The cluster dendrogram of WGCNA. (**D**) The clustered modules of WGCNA. (**E**) Venn diagram of crossover genes plotted against key modular genes.

a pool of free 40s subunits, major pathway of rRNA processing in the nucleolus and cytosol, among others (Figure 6C–G, Supplementary Table 7).

Regulatory Mechanisms of Key Genes

In the TRRUST database, only the biomarker Shh was found being regulates by 16 TFs, including Arx, Cdx2, Gata6, Gbx2, Gli2, Gli3, Msx1, Mtf2, Nfkb1, Nkx2-1, Nr2f2, Pax6, Rela, Six3, Sox2, and Twist1, thereby elucidating their regulatory TF-gene network (Figure 7A). These 16 TFs were significantly enriched in 17 functions, such as diencephalon development and cell fate commitment (Figure 7B). In miRNA-gene network, Ank1 was associated with 21 miRNAs, Cbln4 with 3 miRNAs, L1cam with 18 miRNAs, Gap43 with 9 miRNAs, and Shh with 11 miRNAs (Figure 7C). The

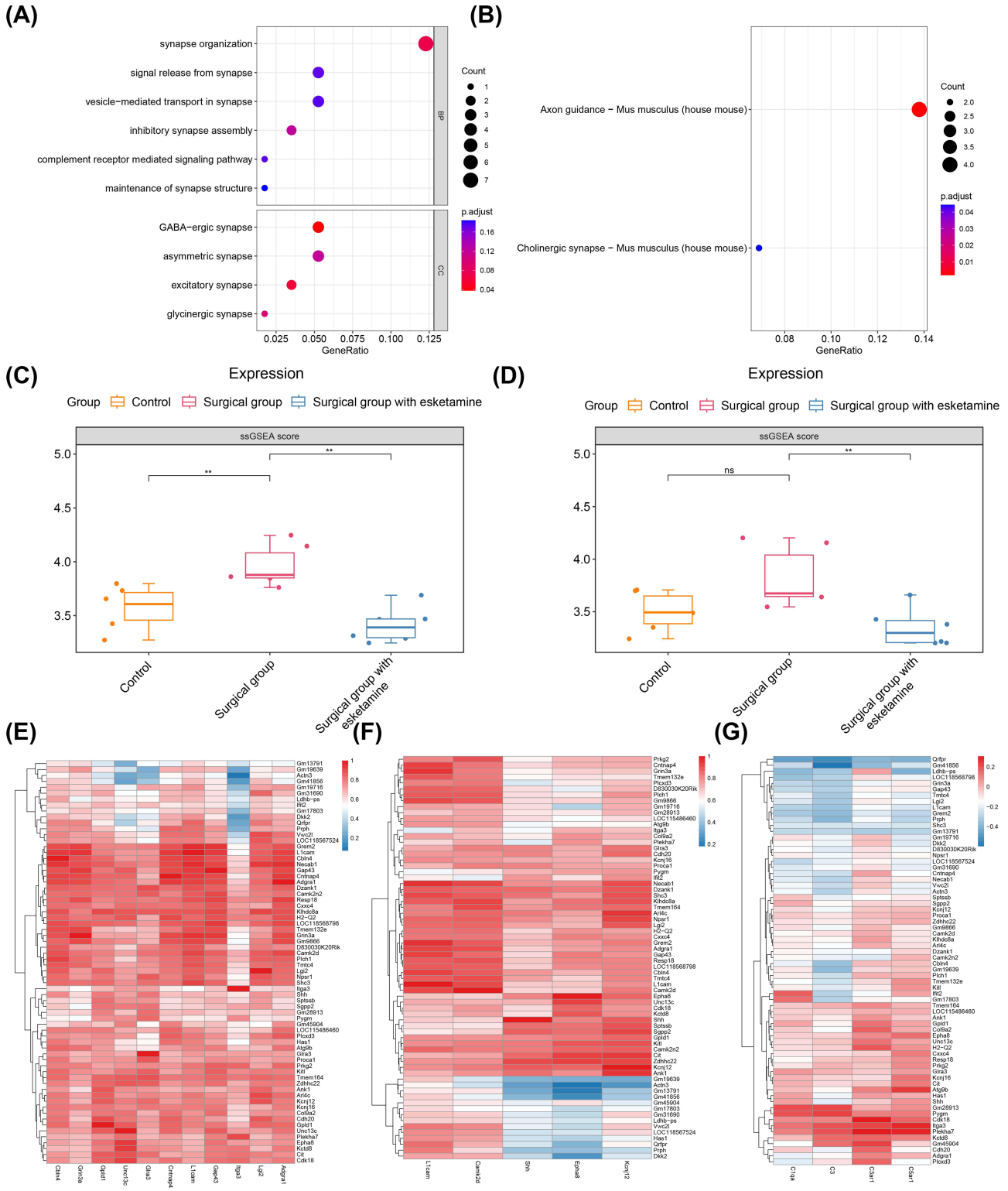

Figure 5 Functional enrichment analysis of candidate genes. (**A**) GO enrichment analysis of the candidate genes. (**B**) KEGG enrichment result of the candidate genes. (**C**) Violin plot of ssGSEA scores for genes in synaptic and complement-related pathways (GO analysis). ** represented $p < 0.01$. The Orange represented the control group, the pink represented the surgical group, and the blue represented the surgical group with esketamine. (**D**) Violin plot of ssGSEA scores for genes in synaptic and complement-related pathways (KEGG analysis). ns represented No significance, ** represented $p < 0.01$. (**E** and **F**) Heatmap of correlations between genes in synaptic and complement-related pathways and candidate genes. (**G**) Heatmap of correlations between complement-related genes (C1qa, C3, C3ar1, C5ar1) and candidate genes. n=6.

https://doi.org/10.2147/DDDT.S510752

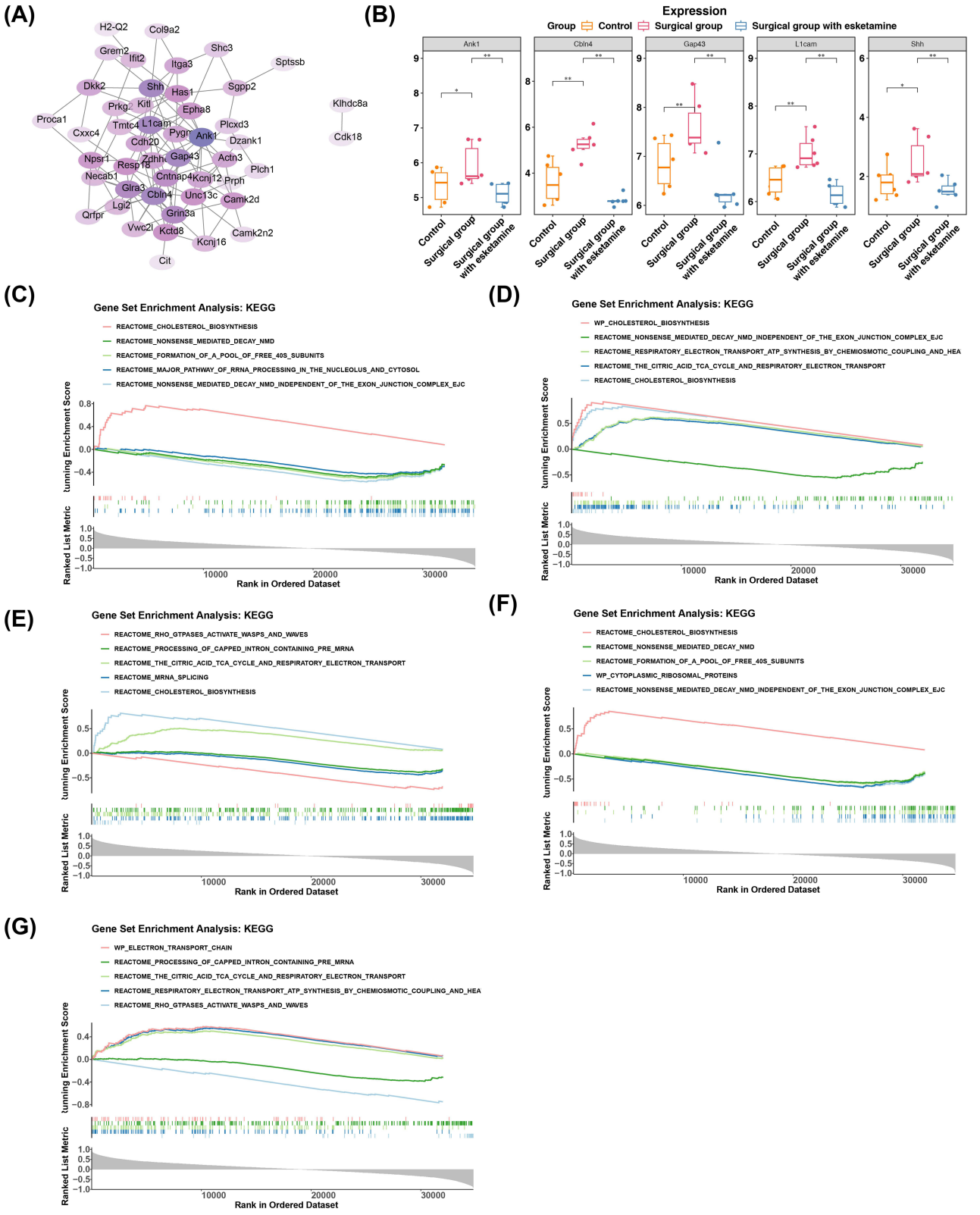

Figure 6 Identification and Gene Set Enrichment Analysis (GSEA) of key genes. (**A**) Protein-protein interaction network of candidate genes. (**B**) Violin plot of expression levels of key genes across different groups. * represented $p < 0.05$, ** represented $p < 0.01$. The Orange represented the control group, the pink represented the surgical group, and the blue represented the surgical group with esketamine. (**C-G**) GSEA of five key genes. The top five broken lines were line graphs of the gene Enrichment Score. The vertical axis was the corresponding Running ES. There was a peak value in the line graph, and this peak value was the Enrichment score of this gene set. The genes before the peak were the core genes in this gene set. The horizontal axis represented each gene in this gene set, corresponding to the vertical lines like barcodes in the second part, and each vertical line corresponded to a gene in this gene set. The third part was the distribution graph of the rank values of all genes. The vertical coordinate was the ranked list metric, and the genes were sorted according to their correlation.

https://doi.org/10.2147/DDDT.S510752

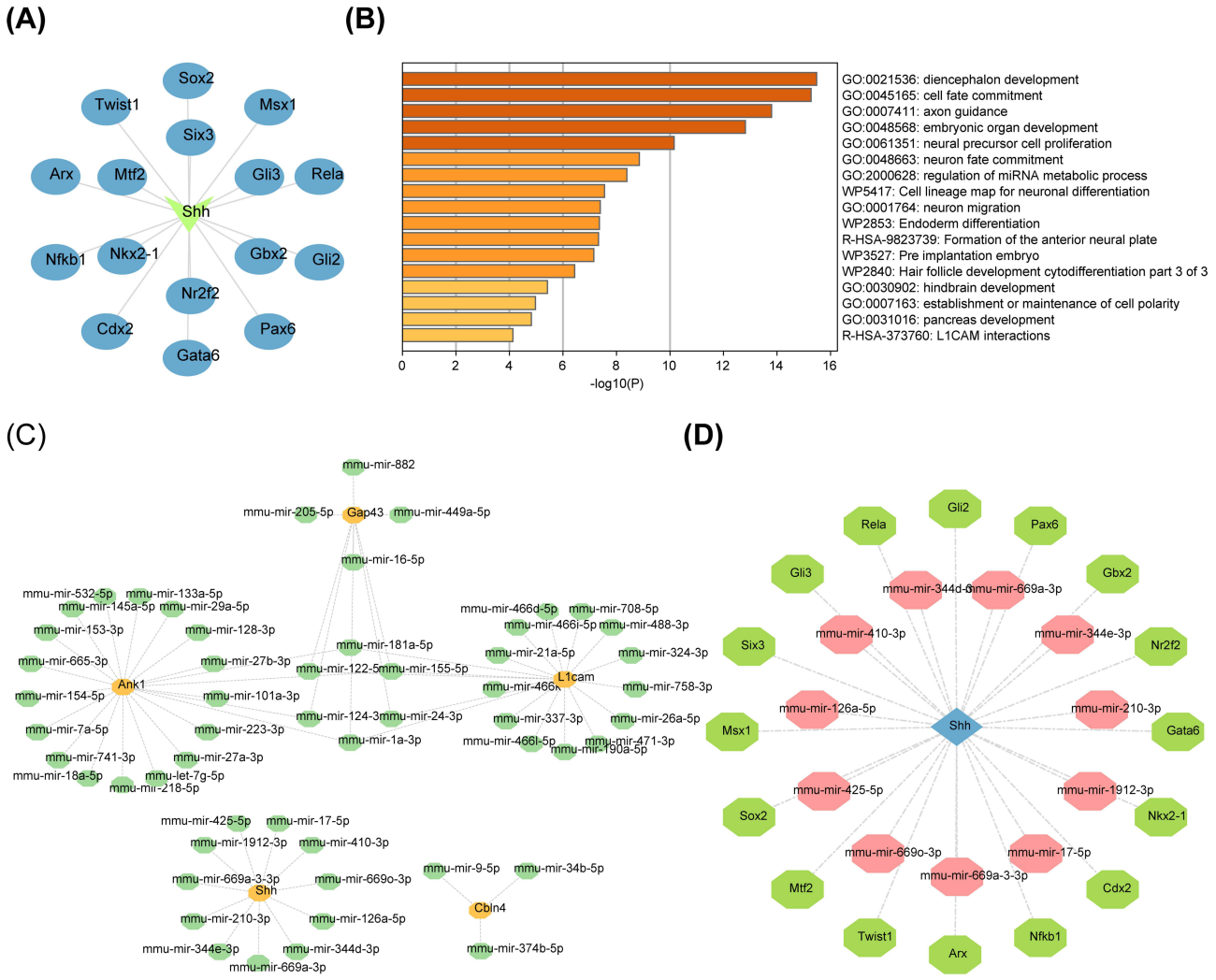

Figure 7 Prediction of regulatory mechanisms for key genes (**A**) Transcription factor-key gene regulatory network. (**B**) Functional enrichment analysis of key genes and transcription factors (TFs). (**C**) miRNA-key gene interaction network. (**D**) miRNA-key gene-TFs network diagram.

miRNAs, mmu-mir-155-5p and mmu-mir-1a-3p, functionally co-regulated the expression of Ank1, Gap43, and L1cam. Additionally, the TF/miRNA-gene regulatory network was depicted, encompassing all 16 TFs and 11 miRNAs (eg mmu-mir-344d-3p and mmu-mir-669a-3p) involved in the regulation of the Shh (Figure 7D).

Expression Verification of Key Genes

The RT-qPCR results demonstrated a upregulation of all key genes in the surgical group, which was subsequently restored to normal levels in the surgical group with esketamine (Figure 8A-E). Specifically, there were notable differences observed in Cbln4, L1cam, and Shh expression between the control and surgical groups. In addition, although there were no significant changes in the expression levels of Ank1 and Gap43 compared to the control group, there was an upward trend. Furthermore, there were significant variations in the expression of all key genes between the surgical group with esketamine and surgical groups.

Discussion

PND is a prevalent neurological condition affecting elderly patients during the perioperative period, significantly impeding their recovery and long-term quality of life, and imposing substantial burdens on families and society.[24] Esketamine, an NMDA receptor antagonist, has gained attention for its anti-inflammatory properties and potential

https://doi.org/10.2147/DDDT.S510752

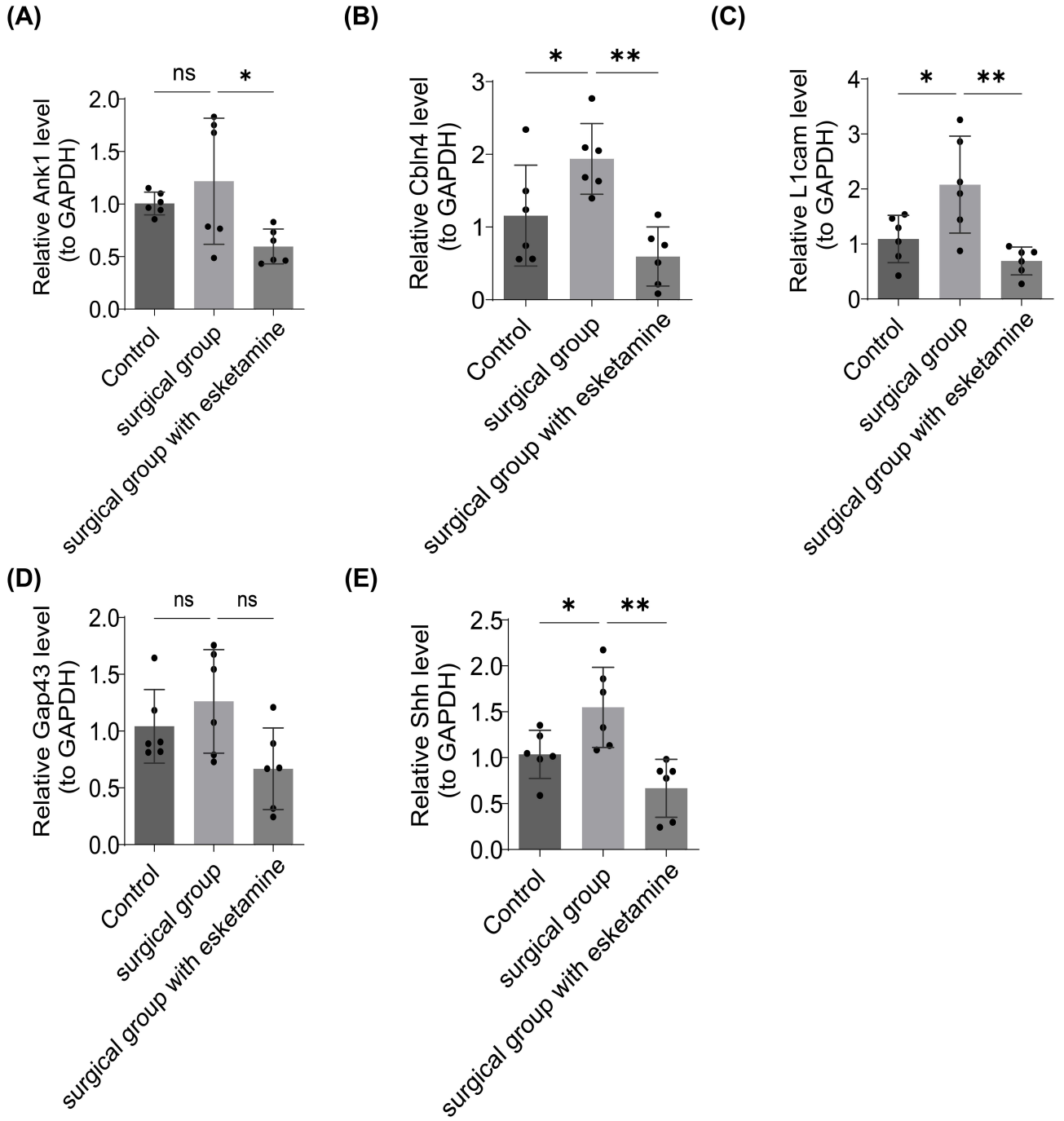

Figure 8 Validation of expression of the mRNA of five hub genes. (**A-E**) qRT-PCR validation of Ank1, Clbn4, L1cam, Gap43 and Shh. ns represented No significance, * represented $p < 0.05$, ** represented $p < 0.01$, n=6.

efficacy in mitigating PND.[25] However, the precise mechanisms underlying its effects are not yet fully understood. In this study, esketamine was used to address sevoflurane-induced PND in elderly mice, followed by an extensive analysis of hippocampal transcriptomic data. We initially identified 557 intersecting genes related to PND treatment from DEGs and analyzed their biological functions and pathways. Through WGCNA, PPI network analysis, functional enrichment, and miRNA network construction, we identified five key genes (Ank1, Cbln4, L1cam, Gap43, and Shh). Their expression levels and trends were validated by qRT-PCR.

The results of the GSEA enrichment analysis showed that the GPCRS non-odorant pathway is upregulated in DEGs1 and downregulated in DEGs2. G protein-coupled receptors (GPCRs) are the largest family of cell surface receptors, characterized by seven transmembrane domains, with approximately 34% of marketed drugs targeting them.[26] The GPCRS non-odorant subclass represents about 90% of GPCRs expressed in the brain. These receptors are crucial for regulating mood, appetite, pain, vision, immune response, cognition, and synaptic transmission, making them promising drug targets for neurological and psychiatric disorders, such as Alzheimer's disease, Parkinson's disease, and Huntington's disease.[27–29] Recent studies have highlighted the significant role of GPCRs in PND development. For instance, Qi et al[30] demonstrated that M1-type microglia can release extracellular vesicles that induce neuroinflammation through the CCR5 - GPCRs - RAS - MAPK pathway, leading to reduced synaptic integrity and worsened cognitive deficits in mice, with GPCRs acting as critical mediators in this process. Moreover, Wen et al[31] found that acetate can reduce microglial activity and neuroinflammation, mitigating PND in mice by binding to GPCR43. These findings support our results. Additionally, research has indicated that GPCRs can serve as functional targets for ketamine's anesthetic effects, suggesting a potential interaction between esketamine and GPCRs.[32] Therefore, the GPCR non-odorant pathway may also become a potential drug target for esketamine in the treatment of PND.

The hippocampus is essential for learning, memory, and emotional regulation, with hippocampal neurons transmitting information through synapses being crucial to these functions.[33] Synapses serve as the neural basis for learning and memory formation.[34] In this study, we identified multiple intersecting genes related to PND treatment from DEGs1 and DEGs2 and explored the neuro-morphological and pathological basis of esketamine's effect on PND using GO and KEGG enrichment analyses. Both KEGG pathway enrichment and GO enrichment analyses robustly indicated that the majority of these intersecting genes are associated with various synapses or synaptic components, including synapse organization, regulation of synapse structure or activity, maintenance of synapse structure, dopaminergic synapse, cholinergic synapse, axon guidance, and glutamatergic synapse. Suo et al[35] used whole transcriptome sequencing to identify pathological processes in the hippocampus of elderly perioperative mice, revealing enrichment in synapse-related biological processes, similar to our findings. Additionally, numerous studies have demonstrated that reductions in synaptic proteins, such as synaptophysin (SYP) and postsynaptic density protein 95 (PSD-95),[36] microglia-mediated synapse loss,[37,38] synapse formation and structural damage,[39,40] and disruptions in synaptic plasticity[41] are critical pathological factors contributing to the development of PND. These findings support our conclusions. Research shows esketamine treats PND in older mice with sleep disorders by reducing M1 microglia polarization in the hippocampus, activating the BDNF-TrkB pathway, and preserving synaptic proteins (SYP and PSD-95), thus protecting synaptic plasticity.[25] Therefore, the impact on different types of synapses and the protection of synaptic plasticity may be key mechanisms by which esketamine treats PND.

This study identified 68 candidate genes associated with esketamine treatment for PND through WGCNA. GO and KEGG analyses revealed significant enrichment in various synaptic types and components, including synapse organization, inhibitory synapse assembly, glycinergic synapses, axon guidance, and cholinergic synapses. These findings further corroborate our previous conclusions. Synaptic pruning, which involves the removal of superfluous synaptic connections, is crucial for maintaining synaptic stability and ensuring normal brain function.[42] Microglia, the resident immune cells in the central nervous system, play a vital role in maintaining synaptic plasticity through complement-mediated synaptic pruning,[43] and abnormal activation of microglia can result in excessive synaptic pruning via the classical complement "eat-me" pathway (C1q/C3-CR3), which is a key mechanism in PND pathogenesis.[44,45] Among the 68 candidate genes, we identified 11 (Cbln4, Grin3a, Gpld1, Unc13c, Glra3, Cntnap4, L1cam, Gap43, Itga3, Lgi2, and Adgra1) that are associated with synaptic and complement-related pathways, showing significant expression differences between the surgical group and surgical group with esketamine. Additionally, Itga3 and Cdk18 exhibit strong correlations with complement-related genes. Therefore, genes and pathways related to synaptic pruning and complement may play a key role in the treatment of PND with esketamine.

Subsequently, through PPI analysis, five key genes involved in esketamine treatment for PND were identified: Ank1, Cbln4, L1cam, Gap43, and Shh. Ank1, a crucial scaffold protein, affects the structure and function of multi-protein complexes.[46] In the CNS, microglia are the source of Ank1 and are associated with microglial activation and movement.[47] Recent studies reveal that elevated Ank1 methylation is a significant risk factor for AD.[48,49]

Furthermore, Ank1 high methylation promotes abnormal microglial activation through enhanced mTOR and STAT3 signaling, leading to immune responses and neuroinflammation, which accelerate AD progression.[49] Importantly, abnormal activation of microglia is a common pathological mechanism in both AD and PND, with overactivated microglia contributing to PND through the promotion of neuroinflammation and excessive synaptic pruning.[50] Our research is the first to identify a link between Ank1 and PND, demonstrating that Ank1 is downregulated after treatment with esketamine. This indicates that esketamine treatment for PND might be related to Ank1 methylation and the synaptic pruning following the abnormal activation of microglia induced by Ank1. Cerebellin 4 (Cbln4) is a secreted synaptic cell adhesion protein widely expressed in the brain, essential for synapse formation, maintenance, and function.[51] Long-term potentiation (LTP), which enhances synaptic strength and plasticity, is critical for learning and memory.[52] In the entorhinal cortex, Cbln4 binds with neogenin-1 to guide axon development, underscoring its role in synaptic plasticity.[53] Balancing excitatory and inhibitory synapses is crucial for sensory processing, motor functions, and cognition, and imbalances often signal neuronal damage and cell death, typical in neurodegenerative diseases like AD.[54,55] Studies show that Cbln4 is responsible for encoding the formation of inhibitory synapses and can interact trans-synaptically with GluD1 in NMDA receptors to jointly regulate inhibitory synapses.[56,57] Our research is the first to establish a link between Cbln4 and esketamine in the treatment of PND. Zou et al 's[58] study identified Cbln4 as a hub gene in AD using WGCNA analysis, which aligns with our findings. In summary, the therapeutic effect of esketamine on PND may be associated with Cbln4's regulatory role in synaptic plasticity or its influence on the balance between excitatory and inhibitory synapses. L1cam, an immunoglobulin superfamily adhesion molecule, is essential for nervous system functions, including synapse formation and plasticity.[59] Extracellular vesicles (EVs) transport various molecules, with L1cam emerging as a promising biomarker for diagnosing Alzheimer's disease (AD) and Parkinson's disease (PD) through brain neuronal EVs, and it correlates with the degree of cognitive impairment.[60–64] This study is the first to report increased L1cam expression in the hippocampal tissue of PND mice. L1cam levels in the cerebrospinal fluid of AD patients, suggesting a link between L1cam and AD.[65] Another study also observed increased L1cam in the frontal cortex of AD brain tissue.[59] Furthermore, Chen et al identified L1cam as a potential immune-related central gene for PD,[66] which aligns with our findings. Recent research has shown that L1cam levels can influence the expression of synaptic proteins such as SYP and PSD-95 in AD mouse models.[67] Therefore, the role of L1cam in synaptic plasticity might explain the therapeutic effects of esketamine in treating PND. Gap43 is a presynaptic protein located on the cytoplasmic side of the presynaptic membrane. When phosphorylated by protein kinase C, Gap43 supports axon growth, neural plasticity, and memory formation.[68] In cultured hippocampal neurons, Gap43 co-localizes with the axonal marker tau protein, serving as a biomarker for synaptic dysfunction.[69] Elevated Gap43 levels in the cerebrospinal fluid of AD patients correlate with accelerated tau protein accumulation, cognitive decline, and worsening symptoms, underscoring Gap43's crucial role in synaptic activity and cognitive function.[70–73] This study is the first to confirm increased Gap43 mRNA levels in the hippocampus of PND mice and to identify Gap43 as essential for esketamine treatment. This suggests that modulating hippocampal Gap43 and its effects on synaptic activity and plasticity may be critical for esketamine's therapeutic effects in PND. Sonic Hedgehog (Shh) is pivotal for activating the Shh pathway, providing neuroprotection via the Gli transcription factor, and supporting synaptic regeneration and neural recovery.[74] In hippocampal neurons, Shh signaling influences presynaptic terminal structure and function, thereby regulating synaptic plasticity.[75,76] Abnormalities in the Shh signaling pathway have been linked to neurological disorders such as AD and Parkinson's disease (PD), contributing to oxidative stress, neuronal excitotoxicity, neuroinflammation, apoptosis, and disrupted synaptic plasticity.[74,77,78] This research demonstrated elevated Shh expression in the hippocampal tissue of PND mice. Previous studies have shown increased Shh signaling in the dentate gyrus of rats with postoperative cognitive impairment, which aligns with our findings. Moreover, modulation of the Shh signaling pathway has been reported to suppress synaptic autophagy in the rat hippocampus and enhance cognitive function.[79] Thus, the Shh signaling pathway may also represent a potential mechanism through which esketamine regulates synaptic plasticity and improves PND.

GSEA was employed to further explore the potential pathways and biological functions of the five key genes, revealing overall similar enrichment results. This study demonstrates that these genes are all enriched in the cholesterol biosynthesis pathway. Cholesterol is crucial for brain function and requires precise regulation. Disruptions in brain cholesterol metabolism are associated with neurodegenerative diseases, and cholesterol depletion negatively affects

synaptic vesicle exocytosis, neuronal activity, and synapse formation and maintenance.[80] Additionally, neurodegeneration and cognitive decline are linked to inflammation and lipid accumulation, with cholesterol acting as a key signal from astrocytes that mediates inflammatory interactions between neurons and microglia.[81] Thus, dysregulation of the cholesterol biosynthesis pathway may contribute to the pathology of PND by inducing neuroinflammation and impairing synaptic plasticity. This research found increased activity in the cholesterol metabolism pathway in the disease group, suggesting that esketamine may influence the risk of PND by modulating key genes and the cholesterol metabolism pathway.

To clarify the role of these five key genes in PND, we compared our findings with transcriptome data from other PND studies. Chen et al analyzed high-throughput data from various brain regions in 27 normal and 52 AD subjects (GSE118553 and GSE161355) and identified Gap43 as a crucial gene common to both AD and diabetes-related cognitive impairment (DACA), noting its involvement in synaptic vesicle cycles and GABAergic synaptic pathways.[82] This overlap underscores the critical role of Gap43 in synaptic plasticity and cognitive function, suggesting that it may contribute to a common pathological mechanism across multiple neurodegenerative diseases, including PND, AD, and DACD. However, other key genes identified in our study—Ank1, Cbln4, L1cam, and Shh—have not been reported in previous PND transcriptome studies. This discrepancy may be due to variations in experimental conditions, disease models, and analytical methods. Our study utilized sevoflurane anesthesia to create a mouse model of PND and focused on esketamine's therapeutic effects, differing from some other PND-related transcriptome data. Additionally, we emphasized the potential biological functions and pathways of key genes in synapse regulation, which may expand our understanding of the molecular mechanisms of PND and offers novel therapeutic targets and robust bioinformatics support for the treatment of PND with esketamine.

The present study identified five key genes and potential mechanisms implicated in esketamine treatment for PND. These mechanisms include the drug's effects on the GPCRS non-odorant pathway, its regulation of various synaptic types and synaptic plasticity, and its impact on the cholesterol biosynthesis pathway. However, there are important limitations to acknowledge. First, our research provides only preliminary validation of these key genes in a mouse model of esketamine treatment for PND. To thoroughly understand the underlying mechanisms, additional animal and cellular experiments are necessary. Second, the use of a PND mouse model may not fully represent human conditions due to potential interspecies differences. Additionally, regarding the RT-qPCR experimental results, we observed that the differences in the expression of Ank1 and Gap43 genes between the control group and the model group were not significant. This may be attributed to factors such as the small sample size, individual variations, and sample heterogeneity. Therefore, further validation with clinical samples is needed to confirm gene expression and evaluate the effectiveness of esketamine treatment in human PND.

Conclusion

In conclusion, this study utilized transcriptome sequencing and bioinformatics methods to identify and validate the expression of five key genes (Ank1, Cbln4, L1cam, Gap43, and Shh) involved in esketamine treatment for PND. The mechanisms include the GPCRS non-odorant pathway, regulation of various synaptic types and synaptic plasticity, and the cholesterol biosynthesis pathway. This study is the first to explore these key genes and mechanisms in the context of esketamine treatment for PND. The findings may help identify potential therapeutic targets for PND and provide new insights for diagnosing and treating patients with perioperative neurocognitive disorders.

Data Sharing Statement

Data analyzed in this manuscript are publicly available from the Sequence Read Archive (https://dataview.ncbi.nlm.nih.gov/object/PRJNA1155165?reviewer=vbsnj6so1fnmjb72suie94g0j7).

Ethics Approval and Consent to Participate

The animal study protocol was approved by the Animal Ethics Committee of Guizhou Medical University on the Use and Care of Animals of NAME OF INSTITUTE (protocol code 2305211) for studies involving animals. This study also adhered to the ARRIVE guidelines (https:// arriveguidelines.org).

Acknowledgment

Wen Hu, Jieqiong Luo, Hui Li and Yushan Luo are co-first authors of this study.

Author Contributions

All authors made a significant contribution to the work reported, whether that is in the conception, study design, execution, acquisition of data, analysis and interpretation, or in all these areas; took part in drafting, revising or critically reviewing the article; gave final approval of the version to be published; have agreed on the journal to which the article has been submitted; and agree to be accountable for all aspects of the work.

Funding

This work was supported by the National Natural Science Foundation of China (No. 82160224) and Key Laboratory of Anesthesia and Pain Research, Guizhou Medical University [2024] fy003.

Disclosure

The authors declare that they have no competing interests.

References

1. Weiser TG, Haynes AB, Molina G, et al. Estimate of the global volume of surgery in 2012: an assessment supporting improved health outcomes. *Lancet*. 2015;385(Suppl 2):S11. doi:10.1016/S0140-6736(15)60806-6
2. Long Y, Feng X, Liu H, et al. Effects of anesthetic depth on postoperative pain and delirium: a meta-analysis of randomized controlled trials with trial sequential analysis. *Chin Med J*. 2022;135(23):2805–2814. doi:10.1097/CM9.0000000000002449
3. Evered LA, Silbert BS. Postoperative cognitive dysfunction and noncardiac surgery. *Anesth Analg*. 2018;127(2):496–505. doi:10.1213/ANE.0000000000003514
4. Evered L, Silbert B, Knopman DS, et al. Recommendations for the nomenclature of cognitive change associated with anaesthesia and surgery-2018. *Br J Anaesth*. 2018;121(5):1005–1012. doi:10.1016/j.bja.2017.11.087
5. Subramaniyan S, Terrando N. Neuroinflammation and perioperative neurocognitive disorders. *Anesth Analg*. 2019;128(4):781–788. doi:10.1213/ANE.0000000000004053
6. Kong H, Xu LM, Wang DX. Perioperative neurocognitive disorders: a narrative review focusing on diagnosis, prevention, and treatment. *CNS Neurosci Ther*. 2022;28(8):1147–1167. doi:10.1111/cns.13873
7. Yang T, Velagapudi R, Terrando N. Neuroinflammation after surgery: from mechanisms to therapeutic targets. *Nat Immunol*. 2020;21(11):1319–1326. doi:10.1038/s41590-020-00812-1
8. Terrando N, Monaco C, Ma D, et al. Tumor necrosis factor-alpha triggers a cytokine cascade yielding postoperative cognitive decline. *Proc Natl Acad Sci U S A*. 2010;107(47):20518–20522. doi:10.1073/pnas.1014557107
9. Netto MB, de Oliveira Junior AN, Goldim M, et al. Oxidative stress and mitochondrial dysfunction contributes to postoperative cognitive dysfunction in elderly rats. *Brain Behav Immun*. 2018;73:661–669. doi:10.1016/j.bbi.2018.07.016
10. Lee C, Jones TA. Effects of ketamine compared with urethane anesthesia on vestibular sensory evoked potentials and systemic physiology in mice. *J Am Assoc Lab Anim Sci*. 2018;57(3):268–277. doi:10.30802/AALAS-JAALAS-17-000131
11. Tu W, Yuan H, Zhang S, et al. Influence of anesthetic induction of propofol combined with esketamine on perioperative stress and inflammatory responses and postoperative cognition of elderly surgical patients. *Am J Transl Res*. 2021;13(3):1701–1709.
12. Ma J, Wang F, Wang J, et al. The effect of low-dose esketamine on postoperative neurocognitive dysfunction in elderly patients undergoing general anesthesia for gastrointestinal tumors: a randomized controlled trial. *Drug Des Devel Ther*. 2023;17:1945–1957. doi:10.2147/DDDT.S406568
13. Han C, Ji H, Guo Y, et al. Effect of subanesthetic dose of esketamine on perioperative neurocognitive disorders in elderly undergoing gastrointestinal surgery: a randomized controlled trial. *Drug Des Devel Ther*. 2023;17:863–873. doi:10.2147/DDDT.S401161
14. Xu G, Wang Y, Chen Z, et al. Esketamine improves propofol-induced brain injury and cognitive impairment in rats. *Transl Neurosci*. 2022;13(1):430–439. doi:10.1515/tnsci-2022-0251
15. Li Y, Wu Z-Y, Zheng W-C, et al. Esketamine alleviates postoperative cognitive decline via stimulator of interferon genes/ TANK-binding kinase 1 signaling pathway in aged rats. *Brain Res Bull*. 2022;187:169–180. doi:10.1016/j.brainresbull.2022.07.004
16. Yang C, Shirayama Y, Zhang J-C, et al. R-ketamine: a rapid-onset and sustained antidepressant without psychotomimetic side effects. *Transl Psychiatry*. 2015;5(9):e632. doi:10.1038/tp.2015.136
17. Love MI, Huber W, Anders S. Moderated estimation of fold change and dispersion for RNA-seq data with DESeq2. *Genome Biol*. 2014;15(12):550. doi:10.1186/s13059-014-0550-8
18. Gustavsson EK, Zhang D, Reynolds RH, et al. ggtranscript: an R package for the visualization and interpretation of transcript isoforms using ggplot2. *Bioinformatics*. 2022;38(15):3844–3846. doi:10.1093/bioinformatics/btac409
19. Gu Z, Hübschmann D. Make Interactive Complex Heatmaps in R. *Bioinformatics*. 2022;38(5):1460–1462. doi:10.1093/bioinformatics/btab806
20. Langfelder P, Horvath S. WGCNA: an R package for weighted correlation network analysis. *BMC Bioinf*. 2008;9:559. doi:10.1186/1471-2105-9-559
21. Wu T, Hu E, Xu S, et al. clusterProfiler 4.0: a universal enrichment tool for interpreting omics data. *Innovation*. 2021;2(3):100141. doi:10.1016/j.xinn.2021.100141

22. Shannon P, Markiel A, Ozier O, et al. Cytoscape: a software environment for integrated models of biomolecular interaction networks. *Genome Res*. 2003;13(11):2498–2504. doi:10.1101/gr.1239303
23. Robles-Jimenez LE, Aranda-Aguirre E, Castelan-Ortega OA, et al. Worldwide traceability of antibiotic residues from livestock in wastewater and soil: a systematic review. *Animals*. 2021;12(1):60. doi:10.3390/ani12010060
24. Lin D, Liu J, Florveus A, et al. Exposure to sevoflurane, but not ketamine, during early-life brain development has long-lasting effects on GABA(A) receptor mediated inhibitory neurotransmission. *Neuroscience*. 2021;472:116–127. doi:10.1016/j.neuroscience.2021.08.001
25. Wen Y, Xu J, Shen J, et al. Esketamine prevents postoperative emotional and cognitive dysfunction by suppressing microglial M1 polarization and regulating the BDNF-TrkB pathway in ageing rats with preoperative sleep disturbance. *mol Neurobiol*. 2024;61(8):5680–5698. doi:10.1007/s12035-023-03860-4
26. Komatsu H. Novel therapeutic GPCRs for psychiatric disorders. *Int J mol Sci*. 2015;16(6):14109–14121. doi:10.3390/ijms160614109
27. Overington JP, Al-Lazikani B, Hopkins AL. How many drug targets are there? *Nat Rev Drug Discov*. 2006;5(12):993–996. doi:10.1038/nrd2199
28. Huang Y, Todd N, Thathiah A. The role of GPCRs in neurodegenerative diseases: avenues for therapeutic intervention. *Curr Opin Pharmacol*. 2017;32:96–110. doi:10.1016/j.coph.2017.02.001
29. Azam S, Haque ME, Jakaria M, et al. G-protein-coupled receptors in CNS: a potential therapeutic target for intervention in neurodegenerative disorders and associated cognitive deficits. *Cells*. 2020;9(2):506. doi:10.3390/cells9020506
30. Qi Z, Peng J, Wang H, et al. Modulating neuroinflammation and cognitive function in postoperative cognitive dysfunction via CCR5 - GPCRs -Ras-MAPK pathway targeting with microglial EVs. *CNS Neurosci Ther*. 2024;30(8):e14924. doi:10.1111/cns.14924
31. Wen C, Xie T, Pan K, et al. Acetate attenuates perioperative neurocognitive disorders in aged mice. *Aging*. 2020;12(4):3862–3879. doi:10.18632/aging.102856
32. Ho J, Perez-Aguilar JM, Gao L, et al. Molecular recognition of ketamine by a subset of olfactory G protein-coupled receptors. *Sci Signal*. 2015;8(370):ra33. doi:10.1126/scisignal.2005912
33. Ayhan F, Kulkarni A, Berto S, et al. Resolving cellular and molecular diversity along the hippocampal anterior-to-posterior axis in humans. *Neuron*. 2021;109(13):2091–2105.e6. doi:10.1016/j.neuron.2021.05.003
34. Ni Y, Feng Y, Shen D, et al. Anti-IgLON5 antibodies cause progressive behavioral and neuropathological changes in mice. *J Neuroinflamm*. 2022;19(1):140. doi:10.1186/s12974-022-02520-z
35. Suo Z, Yang J, Zhou B, et al. Whole-transcriptome sequencing identifies neuroinflammation, metabolism and blood-brain barrier related processes in the hippocampus of aged mice during perioperative period. *CNS Neurosci Ther*. 2022;28(10):1576–1595. doi:10.1111/cns.13901
36. Zhang C, Han Y, Liu X, et al. Odor enrichment attenuates the anesthesia/surgery-induced cognitive impairment. *Ann Surg*. 2023;277(6):e1387–e1396. doi:10.1097/SLA.0000000000005599
37. Yang D, Sun Y, Lin D, et al. Interleukin-33 ameliorates perioperative neurocognitive disorders by modulating microglial state. *Neuropharmacology*. 2024;253:109982. doi:10.1016/j.neuropharm.2024.109982
38. Xu F, Han L, Wang Y, et al. Prolonged anesthesia induces neuroinflammation and complement-mediated microglial synaptic elimination involved in neurocognitive dysfunction and anxiety-like behaviors. *BMC Med*. 2023;21(1):7. doi:10.1186/s12916-022-02705-6
39. Yang Y, Liu Y, Zhu J, et al. Neuroinflammation-mediated mitochondrial dysregulation involved in postoperative cognitive dysfunction. *Free Radic Biol Med*. 2022;178:134–146. doi:10.1016/j.freeradbiomed.2021.12.004
40. Dong R, Han Y, Jiang L, et al. Connexin 43 gap junction-mediated astrocytic network reconstruction attenuates isoflurane-induced cognitive dysfunction in mice. *J Neuroinflamm*. 2022;19(1):64. doi:10.1186/s12974-022-02424-y
41. Xue Z, Shui M, Lin X, et al. Role of BDNF/ProBDNF imbalance in postoperative cognitive dysfunction by modulating synaptic plasticity in aged mice. *Front Aging Neurosci*. 2022;14:780972. doi:10.3389/fnagi.2022.780972
42. Paolicelli RC, Bolasco G, Pagani F, et al. Synaptic pruning by microglia is necessary for normal brain development. *Science*. 2011;333(6048):1456–1458. doi:10.1126/science.1202529
43. Tang S, Hu W, Zou H, et al. The complement system: a potential target for the comorbidity of chronic pain and depression. *Korean J Pain*. 2024;37(2):91–106. doi:10.3344/kjp.23284
44. Tan X, Wang J, Yao J, et al. Microglia participate in postoperative cognitive dysfunction by mediating the loss of inhibitory synapse through the complement pathway. *Neurosci Lett*. 2023;796:137049. doi:10.1016/j.neulet.2023.137049
45. Xiong C, Liu J, Lin D, et al. Complement activation contributes to perioperative neurocognitive disorders in mice. *J Neuroinflamm*. 2018;15(1):254. doi:10.1186/s12974-018-1292-4
46. Kurochkina N, Bhaskar M, Yadav SP, et al. Phosphorylation, dephosphorylation, and multiprotein assemblies regulate dynamic behavior of neuronal cytoskeleton: a mini-review. *Front Mol Neurosci*. 2018;11:373. doi:10.3389/fnmol.2018.00373
47. Delgado-Morales R, Esteller M. Opening up the DNA methylome of dementia. *mol Psychiatry*. 2017;22(4):485–496. doi:10.1038/mp.2016.242
48. Yang Z, Kuboyama T, Tohda C. A systematic strategy for discovering a therapeutic drug for Alzheimer's disease and its target molecule. *Front Pharmacol*. 2017;8:340. doi:10.3389/fphar.2017.00340
49. Morris G, Berk M, Maes M, et al. Could Alzheimer's disease originate in the periphery and if so how so? *Mol Neurobiol*. 2019;56(1):406–434. doi:10.1007/s12035-018-1092-y
50. Harry GJ. Microglia during development and aging. *Pharmacol Ther*. 2013;139(3):313–326. doi:10.1016/j.pharmthera.2013.04.013
51. Seigneur E, Südhof TC. Genetic ablation of all cerebellins reveals synapse organizer functions in multiple regions throughout the brain. *J Neurosci*. 2018;38(20):4774–4790. doi:10.1523/JNEUROSCI.0360-18.2018
52. Gu QH, Yu D, Hu Z, et al. miR-26a and miR-384-5p are required for LTP maintenance and spine enlargement. *Nat Commun*. 2015;6:6789. doi:10.1038/ncomms7789
53. Liakath-Ali K, Polepalli JS, Lee S-J, et al. Transsynaptic cerebellin 4-neogenin 1 signaling mediates LTP in the mouse dentate gyrus. *Proc Natl Acad Sci U S A*. 2022;119(20):e2123421119. doi:10.1073/pnas.2123421119
54. Lin Y, Bloodgood BL, Hauser JL, et al. Activity-dependent regulation of inhibitory synapse development by Npas4. *Nature*. 2008;455(7217):1198–1204. doi:10.1038/nature07319
55. Chacón PJ, Del Marco Á, Arévalo Á, et al. Cerebellin 4, a synaptic protein, enhances inhibitory activity and resistance of neurons to amyloid-β toxicity. *Neurobiol Aging*. 2015;36(2):1057–1071. doi:10.1016/j.neurobiolaging.2014.11.006
56. Hrvatin S, Hochbaum DR, Nagy MA, et al. Single-cell analysis of experience-dependent transcriptomic states in the mouse visual cortex. *Nat Neurosci*. 2018;21(1):120–129. doi:10.1038/s41593-017-0029-5

57. Fossati M, Assendorp N, Gemin O, et al. Trans-synaptic signaling through the glutamate receptor delta-1 mediates inhibitory synapse formation in cortical pyramidal neurons. *Neuron*. 2019;104(6):1081–1094.e7. doi:10.1016/j.neuron.2019.09.027
58. Zou D, Li R, Huang X, et al. Identification of molecular correlations of RBM8A with autophagy in Alzheimer's disease. *Aging*. 2019;11 (23):11673–11685. doi:10.18632/aging.102571
59. Chen S, Jiang Q, Huang P, et al. The L1 cell adhesion molecule affects protein kinase D1 activity in the cerebral cortex in a mouse model of Alzheimer's disease. *Brain Res Bull*. 2020;162:141–150. doi:10.1016/j.brainresbull.2020.06.004
60. Li D, Zou S, Huang Z, et al. Isolation and quantification of L1CAM-positive extracellular vesicles on a chip as a potential biomarker for parkinson's disease. *J Extracell Vesicles*. 2024;13(6):e12467. doi:10.1002/jev2.12467
61. Jiang C, Hopfner F, Berg D, et al. Validation of α-synuclein in L1CAM -immunocaptured exosomes as a biomarker for the stratification of parkinsonian syndromes. *Mov Disord*. 2021;36(11):2663–2669. doi:10.1002/mds.28591
62. Cantres-Rosario YM, Wojna V, Ruiz R, et al. Soluble insulin receptor levels in plasma, exosomes, and urine and its association with HIV-associated neurocognitive disorders. *Front Neurol*. 2022;13:809956. doi:10.3389/fneur.2022.809956
63. Eren E, Leoutsakos J-M, Troncoso J, et al. Neuronal-derived EV biomarkers track cognitive decline in Alzheimer's disease. *Cells*. 2022;11(3):436. doi:10.3390/cells11030436
64. Badhwar A, Hirschberg Y, Valle-Tamayo N, et al. Assessment of brain-derived extracellular vesicle enrichment for blood biomarker analysis in age-related neurodegenerative diseases: an international overview. *Alzheimers Dement*. 2024;20(7):4411–4422. doi:10.1002/alz.13823
65. Strekalova H, Buhmann C, Kleene R, et al. Elevated levels of neural recognition molecule L1 in the cerebrospinal fluid of patients with Alzheimer disease and other dementia syndromes. *Neurobiol Aging*. 2006;27(1):1–9. doi:10.1016/j.neurobiolaging.2004.11.013
66. Chen L, Wang Y, Huang J, et al. Identification of immune-related hub genes in parkinson's disease. *Front Genet*. 2022;13:914645. doi:10.3389/fgene.2022.914645
67. Wang R, Kang S, Zhao Z, et al. Chicoric acid ameliorated beta-amyloid pathology and enhanced expression of synaptic-function-related markers via L1CAM in Alzheimer's disease models. *Int J mol Sci*. 2024;25(6):3408.
68. Ng SC, de la Monte SM, Conboy GL, et al. Cloning of human GAP-43: growth association and ischemic resurgence. *Neuron*. 1988;1(2):133–139. doi:10.1016/0896-6273(88)90197-3
69. Morita S, Miyata S. Synaptic localization of growth-associated protein 43 in cultured hippocampal neurons during synaptogenesis. *Cell Biochem Funct*. 2013;31(5):400–411. doi:10.1002/cbf.2914
70. Franzmeier N, Dehsarvi A, Steward A, et al. Elevated CSF GAP-43 is associated with accelerated tau accumulation and spread in Alzheimer's disease. *Nat Commun*. 2024;15(1):202. doi:10.1038/s41467-023-44374-w
71. Zhu Y, Guo X, Zhu F, et al. Association of CSF GAP-43 and APOE ε4 with cognition in mild cognitive impairment and Alzheimer's disease. *Cells*. 2022;12(1):13. doi:10.3390/cells12010013
72. Sandelius Å, Portelius E, Källén Å, et al. Elevated CSF GAP-43 is Alzheimer's disease specific and associated with tau and amyloid pathology. *Alzheimers Dement*. 2019;15(1):55–64. doi:10.1016/j.jalz.2018.08.006
73. Öhrfelt A, Benedet AL, Ashton NJ, et al. Association of CSF GAP-43 with the rate of cognitive decline and progression to dementia in amyloid-positive individuals. *Neurology*. 2023;100(3):e275–e285. doi:10.1212/WNL.0000000000201417
74. Prajapati A, Mehan S, Khan Z. The role of Smo-Shh/Gli signaling activation in the prevention of neurological and ageing disorders. *Biogerontology*. 2023;24(4):493–531. doi:10.1007/s10522-023-10034-1
75. Dobbs R, Kalmanek E, Choe S, et al. Sonic hedgehog regulation of cavernous nerve regeneration and neurite formation in aged pelvic plexus. *Exp Neurol*. 2019;312:10–19. doi:10.1016/j.expneurol.2018.11.001
76. Ding S, Yang J, Huang X, et al. Dopamine burden induced the inactivation of sonic hedgehog signaling to cognitive decline in minimal hepatic encephalopathy. *Aging Dis*. 2017;8(4):442–457. doi:10.14336/AD.2016.1123
77. Parashar A, Jha D, Mehta V, et al. Sonic hedgehog signalling pathway contributes in age-related disorders and Alzheimer's disease. *Ageing Res Rev*. 2024;96:102271. doi:10.1016/j.arr.2024.102271
78. Schmidt S, Luecken MD, Trümbach D, et al. Primary cilia and SHH signaling impairments in human and mouse models of parkinson's disease. *Nat Commun*. 2022;13(1):4819. doi:10.1038/s41467-022-32229-9
79. Li PJ, Guo Y-Q, Ding P-Y, et al. Neuroprotective effects of a smoothened receptor agonist against postoperative cognitive dysfunction by promoting autophagy in the dentate gyrus of aged rats. *Neurol Res*. 2019;41(10):867–874. doi:10.1080/01616412.2019.1628411
80. Zhang J, Liu Q. Cholesterol metabolism and homeostasis in the brain. *Protein Cell*. 2015;6(4):254–264. doi:10.1007/s13238-014-0131-3
81. Hansen SB, Wang H. The shared role of cholesterol in neuronal and peripheral inflammation. *Pharmacol Ther*. 2023;249:108486. doi:10.1016/j.pharmthera.2023.108486
82. Chen Y, Ji X, Bao Z. Identification of the shared gene signatures between Alzheimer's disease and diabetes-associated cognitive dysfunction by bioinformatics analysis combined with biological experiment. *J Alzheimers Dis*. 2024;101(2):611–625. doi:10.3233/JAD-240353